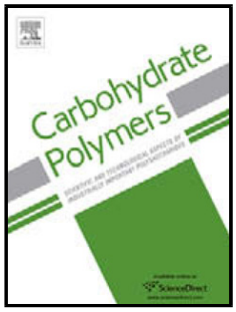

Title: Kinetic and Structural Analysis of Fluorescent Peptides on Cotton Cellulose Nanocrystals as Elastase Sensors

Author: J. Vincent Edwards Nicolette T. Prevost Alfred D. French Monica Concha Brian D. Condon

PII: S0144-8617(14)00424-X
DOI: http://dx.doi.org/doi:10.1016/j.carbpol.2014.04.067
Reference: CARP 8828

To appear in:

Received date: 7-11-2013
Revised date: 18-4-2014
Accepted date: 20-4-2014

Please cite this article as: Edwards, J. V., Prevost, N. T., French, A. D., Concha, M., & Condon, B. D.,Kinetic and Structural Analysis of Fluorescent Peptides on Cotton Cellulose Nanocrystals as Elastase Sensors, *Carbohydrate Polymers* (2014), http://dx.doi.org/10.1016/j.carbpol.2014.04.067

Kinetic and Structural Analysis of Fluorescent Peptides on Cotton Cellulose Nanocrystals as Elastase Sensors

J. Vincent Edwards*, Nicolette T. Prevost, Alfred D. French, Monica Concha, Brian D. Condon

USDA-ARS, Southern Regional Research Center, 1100 Robert E. Lee Blvd., New Orleans, LA 70124

*Corresponding Author
J. Vincent Edwards
Southern Regional Research Center, ARS-USDA
1100 Robert E. Lee Blvd.
New Orleans, LA 70124
vince.edwards@ars.usda.gov
office: 504-286-4360 fax 504-286-4390

Kinetic and Structural Analysis of Fluorescent Peptides on Cotton Cellulose Nanocrystals as Elastase Sensors

J. Vincent Edwards, Nicolette T. Prevost, Alfred D. French, Monica Concha, Brian D. Condon

Abstract

Human neutrophil elastase (HNE) and porcine pancreatic elastase (PPE) are serine proteases with destructive proteolytic activity. Because of this activity, there is considerable interest in elastase sensors. Herein we report the synthesis, characterization, and kinetic profiles of tri- and tetrapeptide substrates of elastase as glycine-esterified fluorescent analogs of cotton cellulose nanocrystals (CCN). The degree of substitution of peptide incorporated in CCN was 3-4 peptides per 100 anhydroglucose units. Glycine and peptide-cellulose-nanocrystals revealed crystallinity indices of 79 and 76 percent respectively, and a crystallite size of 58.5 Å. A crystallite model of the peptide-cellulose conjugate is shown. The tripeptide conjugate of CCN demonstrated five-fold greater efficiency in HNE than the tripeptide in solution judged by its k_{cat}/K_m of 33,515. The sensor limits of detection at 2 mg of the tri- and tetrapeptide CCN conjugates over a 10 minute reaction time course were 0.03 U/mL PPE and 0.05 U/mL HNE respectively.

Keywords: biosensor, human neutrophil elastase, cotton/cellulose, nanocrystals

1. Introduction

1.1 Elastase in Disease and Fluorescent Analog Sensors

Human neutrophil elastase (HNE) and porcine pancreatic elastase (PPE) are serine proteases that contain a conserved triad of catalytic residues and a very nucleophilic active-site serine. They have well-characterized substrate specificities, and mechanism-based inhibitors have been developed (Bode, Meyer & Powers, 1989; Stein, 1983; Yasutake & Powers, 1981). The elastases have long been well characterized for their essential functions against infection (HNE) and digestion (PPE), but when left unchecked they are the source of inflammatory diseases (Boudjelthia, Saulnier & Wallach, 1990; Jaffray, Yang, Carter, Mendez & Norman, 2000; McRae, Nakajima, Travis & Powers, 1980). Elastase and other proteases and oxidative species are associated with prolonged and excessive neutrophil recruitment that is the basis of numerous inflammatory and autoimmune diseases (Caielli, Banchereau & Pascual, 2012; Weiss, 1989). Thus, elastase among other similar serine proteases is a therapeutic target in human disease (Korkmaz, Horwitz, Jenne & Gauthier, 2010), and methods for the sensitive detection of elastases have been of considerable interest. Elastase detection has been explored with sensor motifs utilizing different peptide substrate or protease recognition sequences. In this regard various sensor design motifs employing sensitive fluorescent detection have been reported and recently reviewed, including: 1) A microchip integrated with reagent-release capillaries as a ‘drop-and-sip’ technique, utilizing a single microliter droplet of HNE-containing solution with fluorescence image analysis of the hydrolyzed substrate product (Henares et al., 2006). 2) Fluorometric detection of HNE activity with synthetic supramolecular pore sensors (Das, Talukdar & Matile, 2002; Sorde, Das & Matile, 2003). 3) The covalent immobilization of HNE on biosensor chips having surface plasma resonance capability has also been employed for analysis of HNE inhibitors (Shen, Shimmon, Smith & Ghosh, 2003). 4) More recently we showed how colorimetric peptides anchored to nanocrystalline cellulose sensitively visualize elastase activity, and work well with

cellulose dialysis membranes to filter both chromophore and enzyme for flexible, sensitive detection (Edwards, Prevost, Sethumadhavan, Ullah & Condon, 2013).

1.2 Fluorescent Cellulose Analogs and Peptide Biosensors

The potential to use biosensors constructed of cellulose in the form of microdialysis or ultrafiltration probes has been reviewed (Steuerwald, Villeneuve, Sun & Stenken, 2006). In one biosensor the enzyme is immobilized between two cellulose nitrate filters (Ballerstadt & Schultz, 1996). Another employs a microdialysis sampling assay of HNE activity in which the substrate is delivered through the microdialysis probe to external solutions containing HNE, and the product, *para*-nitroaniline, is recovered back into the probe (Leegsma-Vogt, Rhemrev-Boom, Tiessen, Venema & Korf, 2004).
The attachment of bioactive, fluorescent molecules to CCN has recently been shown to provide numerous pertinent applications (Lam, Male, Chong, Leung & Luong, 2012). For example, nanoparticles within cells can be quantified and localized using positively charged fluorescent CCN for bioimaging, and peptide and enzyme fluorophores can be attached to CCN for biosensing. Also, fluorescent cellulose nanocrystals from flax that were derivatized with rhodamine B or fluorescein-5-isothiocyanate (Mahmoud, Mena, Male, Hrapovic, Kamen & Luong, 2010) have been assessed for cellular imaging. Both the fluorescent CCN analog 1-pyrenebutyryl- 3-aminopropyl-silanized cellulose (Yang & Pan, 2010) and terpyridine-modified pyrylene cellulose, a self assembled supramolecular complex with high affinity for transition metals (Hassan, Moorefield, Elbatal, Newkome, Modarelli & Romano, 2012), have potential for biosensing and imaging applications. Fluorescent coumarin and anthracene analogs of TEMPO oxidized, propargylamino-nanocellulose crystals were also prepared though “Click” chemistry (Filpponen, Sadeghifar & Argyropoulos, 2011).

Although there have been a wide array of uses for synthetic peptides on cellulose (Blackwell, 2006) there have been few reports on nanocrystalline cellulose-peptide conjugates. Fluorescent Tryptophan-containing peptide conjugates of TEMPO oxidized nanocellulose were prepared and retained their fluorescent properties (Barazzouk &

Daneault, 2012). A higher yield general route to peptide conjugation on cellulose surfaces has also been recently disclosed using a xyloglucan-peptide conjugate for activation (Araújo, Nakhai, Ruda, Slättegård, Gatenholm & Brumer, 2012). Intramolecularly quenched fluorogenic substrates of neutrophil serine proteases that distinguish human neutrophil elastase, proteinase 3, and chathepsin G activities at free and membrane bound sub-nanomolar concentrations of HNE have been reported (Korkmaz et al., 2012).

This paper outlines an approach to using cotton cellulose nanocrystalline fluorescent peptide conjugates as a sensitive biosensor for HNE. Previously we discussed the relationship of specific surface area to the DS levels for colorimetric peptide-nanocellulose conjugates, and characterized them in terms of derivatization of available hydroxymethyl groups on the surface of the nanocrystal and the resulting elastase sensitivity (Edwards, Prevost, Sethumadhavan, Ullah & Condon, 2013). Here we examine the kinetic and crystal structure relationship of HNE elastase substrates that are fluorescent peptide conjugates of cellulose nanocrystals as biosensors of HNE.

2. Materials and Methods

2.1 Materials

The substrates n-succinyl-Alanine-Proline-Alanine-4-amido-7-methyl-coumarin (APA-AMC) and n-succinyl-Alanine-Alanine-Proline-Valine-4amido-7-methyl-coumarin (AAPV-AMC) were purchased from Bachem. Human neutrophil elastase was purchased from Athens Research Technologies and porcine pancreatic elastase was purchased from mybiosource.com. Hydroxybenzotriazole (HOBT) was purchased from Sciencelab.com, Inc., Houston, TX. Diisopropylcarbodiimide (DIC) and Oxyma Pure (ethylcyanoglyoxylate-2-oxime) were purchased from Sigma Aldrich, and 9-fluorenylmethoxycarbonyl-glycine (Fmoc-glycine) was purchased from Peptides International, Louisville, KY, USA. Cotton cellulose nanocrystal (CCN) freeze- dried powder was supplied by Dr. Quiglin Wu from Louisiana State University, Baton Rouge,

LA. The cotton filter paper used was Whatman #4 quantitative. All other chemicals were commercial reagent grade and used without further purification.

2.2 Methods

2.2.1 Preparation, and Properties of Cotton Cellulose Nanocrystals (CCN)

CCNs were made using 64% sulfuric acid aqueous solution with a cotton-to-acid weight ratio of 1 to 10 at 45 ºC. The cotton fibers were pre-mixed with the acid and the mixture was stirred vigorously for 1 hour. Immediately following hydrolysis, the suspension was diluted five-fold to stop the reaction. The suspension was then transferred into centrifuge bottles and was centrifuged at 12,000 rpm for 10 min (Sorvall ST-16R, Thermo Fisher Scientific, Portsmouth, NH, USA) and decanted to separate the crystals. The crystals were then washed with distilled water and the mixture was centrifuged again. The process was repeated four to five times for each sample to reduce the acid content. Afterward, regenerated cellulose dialysis tubes (Fisher Scientific, Pittsburgh, PA, USA) with a molecular weight cutoff of 12,000–14,000 Da were used to dialyze the suspension against distilled water until the water pH reached a value of 7.0.

To further disperse and reduce the size of the cellulose fiber fragments, mechanical treatment was applied to the chemically treated samples. The suspension of cellulose crystals was processed through a high-pressure homogenizer (Microfluidizer M-110P, Microfluidics Corp., Newton, MA, USA) equipped with a pair of Z-shaped interaction chambers (one 200 µm ceramic, and one 87 µm diamond) under an operating pressure of 207 MPa. After 10 passes through the high-pressure homogenizer, the suspension was collected and dried using a freeze-dryer (FreeZone, 2.5 plus, Labconco Corp., Kansas City, MO, USA) to obtain dry CCNs. The CCNs were found to be of similar dimensions and charge as previously characterized (Edwards, et al., 2013, Yue, et al., 2012) such that after ten passes of homogenizer the average length was 159+/- 57nm and the average diameter of 15.0+/- 4.5nm, and after freeze drying in preparation for the sensor reactions reported here the length was 700-900 or > 1,000 nm in length and 10-40 nm in diameter.

CCN charge was assessed by measuring the zeta potential using a Malvern Zetasizer Nano ZS90 (Malvern Instruments, Worcestershire, UK). The CCN sample was diluted with deionized water, sonicated for a half hour, and analyzed at a concentration of 1.0 mg/mL. The resulting ζ potential based on three separate determinations was found to be -41.5 mv +/- 1.3 mv-0.5mv.

2.2.2 Esterification of cotton cellulose nanocrystal with Fmoc-glycine

Briefly, the untreated cellulose Iβ CCN (2.0 g, 0.012 mol) was placed in a flask containing Fmoc-glycine (0.012 mol), HOBT (0.012 mol), DIC (0.012 mol) in dimethylformamide (DMF) with dimethylaminopyridine (DMAP) (1.2 mmol). The flask was placed in an ultrasonic ice bath for about an hour. It was then centrifuged at 6000 rpm for 10 minutes to separate the crystals from the reaction mixture. It was then washed with DMF twice and dichloromethane (DCM) twice, each time by vortexing the solid in solvent, and then centrifuging and decanting the solvent. The CCN were dried in air on a watch glass and then stored at ~4-8ºC. Deprotection of the CCN was accomplished by suspending the Fmoc-gly-CCN in a 20% piperidine/DMF solution and sonicating for 5 minutes. It was then washed twice with DMF and then DCM twice, each time using a centrifuge/decant cycle.

2.2.3 Immobilization of elastase substrates on glycine-CCN

To a flask were added DIC (0.68-0.98 mmol), HOBT (0.68-0.98 mmol) or Oxyma Pure(Subirós-Funosas, Prohens, Barbas, El-Faham & Albericio, 2009) (0.68-0.98 mmol) and respective substrate (0.052-0.07 mmol) in minimal DMF. The glycine-cotton CCN powder (0.67-1.0 mmol) was added to this solution and placed in a sonicated ice bath for 2 hrs and then placed in the refrigerator overnight. Afterwards, the samples were separated and washed with DMF and methanol using centrifuge/decant cycles for the nanocrystal. The samples were air dried and stored at 4-8 ºC until further use.

2.2.4 Enzyme Assay for fluorogenic substrate

Stock solutions of the substrate and enzyme were prepared from which subsequent working solutions were made with the phosphate buffer solution (PBS) of 0.1M sodium dihydrogen phosphate (NaH_2PO_4), 0.5 M sodium chloride (NaCl). A standard curve was prepared with simple dilution of stock solution. The first well was filled with 100 µL of substrate stock solution, 1 µmole/mL. The second through eighth wells were filled with

100 µL of buffer. To the second well, 100 µL of stock was added and mixed. One hundred µL of the second was transferred to the third well, mixed and the process continued. From the seventh well, 100 µL was discarded and nothing added to the last yielding a range of 1 to 0.0156 µmole/mL. To start the reaction, 100 µL of porcine elastase solution [3 U/mL] was added to 100 µL of nanocrystal sample stock solution, 20 mg/mL equaling about 2 mg of sample. Measurement commenced immediately at 37 ˚C and continued for 1 h at 1 min intervals. The plate was shaken before each measurement (10 s) and emission was monitored at 460 nm with excitation at 360 nm to measure the increase in fluorescence of the amidolytic activity.

2.2.5 Mass spectroscopy analysis

The samples were analyzed via LC/MS, using an Agilent 1200 LC system, an Agilent Chip-cube interface and an Agilent 6520 Q-TOF tandem mass spectrometer (Agilent Technologies, Santa Clara, CA). Chromatographic separation was accomplished using a Chip consisting of a 40 nL enrichment column and a 43 mm analytical column packed with C18, 5 µm beads with 300A pores. One µl aliquots of the sample were transferred to the enrichment column via the 1200 capillary pump operating at a flow of 4 µl/min. The 1200 nano pump was operated at a flow rate of 600 nL/min. An initial gradient (Solvent A-100% H2O, 0.1% Formic Acid; Solvent B- 90% ACN, 10% H2O and 0.1% Formic Acid) of 97% A was changed to 30% Solvent A at 12 min, 0% at 13 min, 100% at 14 min, 0% at 15 min. A post-run time of 4 min was employed for column equilibration.

The MS source was operated at 300°C with 5 L/min N_2 flow and a fragmentor voltage of 175V. N_2 was used as the collision gas with collision energy varied as a function of mass and charge using a slope of 3.7 V/100 Da and an offset of 2.5 V. Both quad and TOF were operated in positive ion mode. Reference compounds of 322.048121 Da and 1221.990637 Da were continually leaked into the source for mass calibration. An initial MS scan was performed from m/z 300 to 1600 and up to three multiply charged ions were selected for MS/MS analysis.

2.2.6 X-Ray Diffraction

Samples were pressed pellets, scanned in the θ-2θ reflection mode with a Philips X'pert powder diffractometer, a Cu tube and a graphite monochromator. The Crystallinity Index (Segal, Creely, Martin & Conrad, 1959) was determined by subtracting the minimum intensity near 18° 2-θ from the maximum intensity (at 22.87° 2-θ) and dividing the difference by the maximum intensity. No background correction was made. The crystal width was calculated by the Scherrer equation (Scherrer, 1918) with a shape factor of 1.0. Theoretical patterns were calculated with the Debyer software (https://code.google.com/p/debyer/) based on a model consisting of 109 cellulose chains, each 20 glucose residues in length, arranged according to the coordinates of Nishiyama et al. (Nishiyama, Langan & Chanzy, 2002). The model was based on an 11-chain by 11-chain structure (see a similar 12x12 model in (Nishiyama, Johnson & French, 2012), but with six chains removed from the top of the crystal and six from the bottom.

2.2.7 Molecular Model of Peptide-conjugated cellulose nanocrystal

The peptide-conjugated nanocrystal was built using GaussView 5.0 (GaussView, Version 5, Dennington, R.; Keith, T.; Millam, J. Semichem Inc., Shawnee Mission KS, 2009) and visualized with VMD (Visual Molecular Dynamics) software (Humphrey, Dalke & Schulten, 1996). The peptide was optimized using Gaussian 09* using the semi-empirical PM3 method on a Linux cluster. The basic 9-chain nanocrystal was taken from a library of structures (Nishiyama, Johnson & French, 2012) created using the Mercury program (Macrae et al., 2008). Work on addition of peptides to the above much larger 109-chain model and studies with molecular dynamics and simulated diffraction continues.

2.2.8 Kinetic Studies

The rates of hydrolysis of the tri- and tetra-peptide fluorogenic substrates, both free in solution and immobilized on CCN, were measured by monitoring the emission of the released amidomethylcoumarin in buffered solution, 0.1 M NaH_2PO_4 containing 0.5 M NaCl pH 7.6, at 37 ºC. In a typical experiment, 100 µL of the appropriate enzyme solution, 0.5 U/mL, was added to 200 µL of substrate sample solution at 5-6 separate concentrations in three forms: free in solution, immobilized on CCN, and immobilized on filter paper. The increase in fluorescence at 460 nm with excitation at 360 nm was measured for 10 min at 20 s intervals using a microplate reader. The K_m and V_{max} values were calculated using the experimental initial rates and Graph Pad Prism 6 software. Enzyme kinetics was chosen to create XY columns for sample data. After inserting experimental values, data was analyzed selecting nonlinear regression for curve fit, subsequently choosing enzyme kinetics-substrate vs. velocity, Michaelis-Menten to determine the K_m and V_{max} values.

2.2.9 Emission Spectrometry

The emission spectra were measured with a Shimadzu RF5301 spectrofluorometer. Equal amounts of substrate in solution, concentration ranging 0-0.5 µmole/mL, and elastase enzyme were combined totaling 200 µL and allowed to incubate for at least 30 min. at 37 ºC before dilution (15 X) with sodium phosphate buffer for fluorescence measurements. Emission measurements scanned 400-625 nm with excitation at 365 nm. A 2 mg substrate sample was immobilized on the nanocrystals and a 4 mg sample of substrate was immobilized on filter paper. The concentrations of the elastases were 3 U/mL for pancreatic porcine and 2 U/mL for human neutrophil.

3. Results and Discussion

3.1 Synthesis and Characterization

The HNE and PPE substrate analog peptides were covalently attached to CCN as previously reported (Edwards, Prevost, Sethumadhavan, Ullah & Condon, 2013) and

the chemical structures of the peptide-cellulose conjugates are shown in Figure 1. The sulfate-conferred charge of cellulose whiskers enhances dispersion in dimethylformamide (Azizi Samir, Alloin, Sanchez, El Kissi & Dufresne, 2004; Edwards, Prevost, Sethumadhavan, Ullah & Condon, 2013), and the reaction mixtures of the Glycine-CCN ester with the peptide in DMF were visibly clear suspensions. However, as pointed out previously (Edwards, Prevost, Sethumadhavan, Ullah & Condon, 2013) other factors affect the yield besides the reactive peptide-carbodiimide intermediate (used in 1:1 molar ratio in this study)since the DS levels of the peptide incorporation were 3-6 times lower than those of the esterification of glycine to CCN.

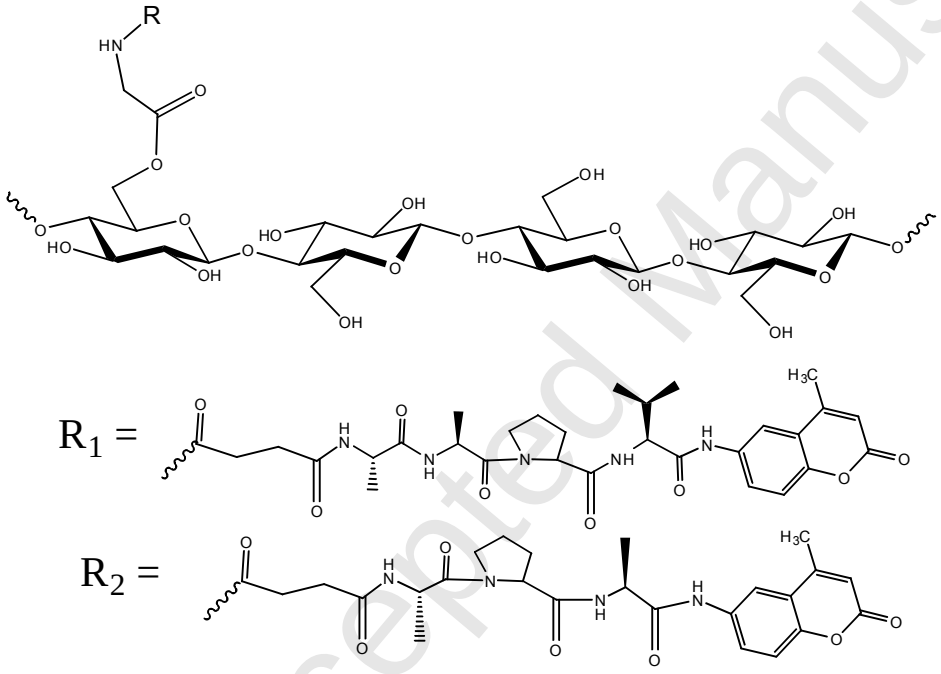

Figure 1

The peptide analogs were characterized with fluorescence scanning, elemental analysis and mass spectroscopy (Table 1). Determinations of peptide titer on CCN were made from fluorescent peptide analogs in solution. As shown in Table I both the fluorescence and elemental analysis reveal that the amount of tripeptide incorporated on CCN was somewhat higher than the tetrapeptide.

Table 1: Characterization values for peptide-cellulose conjugates including elemental analysis, fluorescence emission spectra, and Mass spectroscopy parent ions.

Sample	N%	C%; H%; S%	DS levels calc.	Assay calc. conc.[a] (μmoles/gram of CCN)	Emission calc. conc.[b] (μmoles/gram of CCN)	Mass Spec parent ions[c] (m/z)
Gly-CCN	1.16	41.28; 9.90; 0.24	0.141			
APA-AMC-CCN	1.65	40.04; 8.28; 0.21	0.044	123.5	161.5	572.236
AAPV-AMC-CCN	1.24	40.71; 8.33; 0.25	0.026	29.5	55.6	671.302

[a]Amount of substrate immobilized on nanocrystals calculated after 30 minutes of incubation at 37C with enzyme using 2mg of nanocrystal. [b]Amount of immobilized substrate was calculated from the standard curve of substrate in solution emission at 460nm. The same conditions were used as the assay before diluting for fluorescent measurement. [c] Mass spectroscopy ions include the glycidyl link to attach peptide to nanocrystal (see figure 1).

The DS values shown in Table 1 for peptide nanocrystalline cellulose conjugates were calculated for the Glycine-ester of cellulose (Glycine-CCN) and the peptide-cellulose conjugates (peptide-CCN) based on the method Touzinsky et al. (Touzinsky & Gordon, 1979), which has been shown to be applicable to a variety of cellulose substitutions. The DS level of the Glycine-CCN is 0.141 and for the peptide-CCN 0.03 – 0.04, indicating that approximately 3 – 4 peptides are linked per 100 AGU on the HNE sensor. This substitution is consistent with the previous reports on colorimetric analogs (Edwards, et al., 2013). The D.S. levels are consistent with the assay and fluorescent based calculations of peptide titer attached to CCN. The peptide substitution level, which appears low, is attributed to the synthetic modification taking place primarily at the CCN surfaces, with many of the cellulose molecules being inaccessible because they are in the CCN interior. In the model in Fig. 2, there are a total of 109 chains with 30 chains on the $1\bar{1}0$ and 110 surfaces, and half of the primary alcohol groups on those surface chains are in the interior. Thus, approximately 14% of the total primary hydroxyls are exposed on the crystallite surface. This level of surface primary hydroxyl exposure is consistent with values calculated using methods recently reported for other types of nanocellulose crystallites (Jiang, Han, Hsieh, 2013, Okita, Saito, Isogai, 2010) (The sulfate groups on the surface primary hydroxyls, which result from the use of sulfuric acid hydrolysis to prepare the CCN, occupy roughly 3.6% of the total primary

hydroxyls as determined from elemental analysis (Table 1). It has previously been observed that up to 10 per cent of the primary alcohols may be sulfated on cellulose crystallites (Fleming, Gray, & Matthews, 2001).

This is not so different from the two percent of hydroxymethyl groups of anhydroglucose residues being oriented to exposure at the surfaces of cellulose nanowhiskers (Fleming, Gray & Matthews, 2001). (Lam, Male, Chong, Leung & Luong, 2012). However, the benefit of the greater surface area of nanocrystalline cellulose has been well documented (Eyley & Thielemans, 2011; Habibi, Chanzy & Vignon, 2006; Siqueira, Bras & Dufresne, 2009), and the benefit of surface exposed peptides in this study is proven by the good results in kinetic profile as discussed below. DS determinations have previously been made for the determination of surface area of nanocrystalline cellulose using a variety of methods (Castillo, Nakajima, Zimmerman & Powers, 1979; Eyley & Thielemans, 2011; Siqueira, Bras & Dufresne, 2009). For example DS levels of surface hydroxymethyl groups (a DS of 0.09) are considered stoichiometric for TEMPO oxidized nanocellulose (Castillo, Nakajima, Zimmerman & Powers, 1979). Hence the substitution levels observed for the types of modifications reported here appear reasonable.

X-ray diffraction patterns of the Gly-CCN and peptide-CCN are shown in Figure 3. These nanocrystalline preparations are identified as cellulose I by their diffraction patterns, with three peaks at 2-θ for cellulose I (2-θ = 14.74°, 16.60°, and 22.87°). Glycine and peptide-cellulose-nanocrystals revealed crystallinity indices of 79 and 76 percent respectively ` The X-ray diffraction of the peptide-cellulose nanocrystalline conjugates are expected to experience additional scattering from the peptide content. Based on the crystallite size measured by the Scherrer formula (Scherrer, 1918), the crystallite width was 58.5 Å.

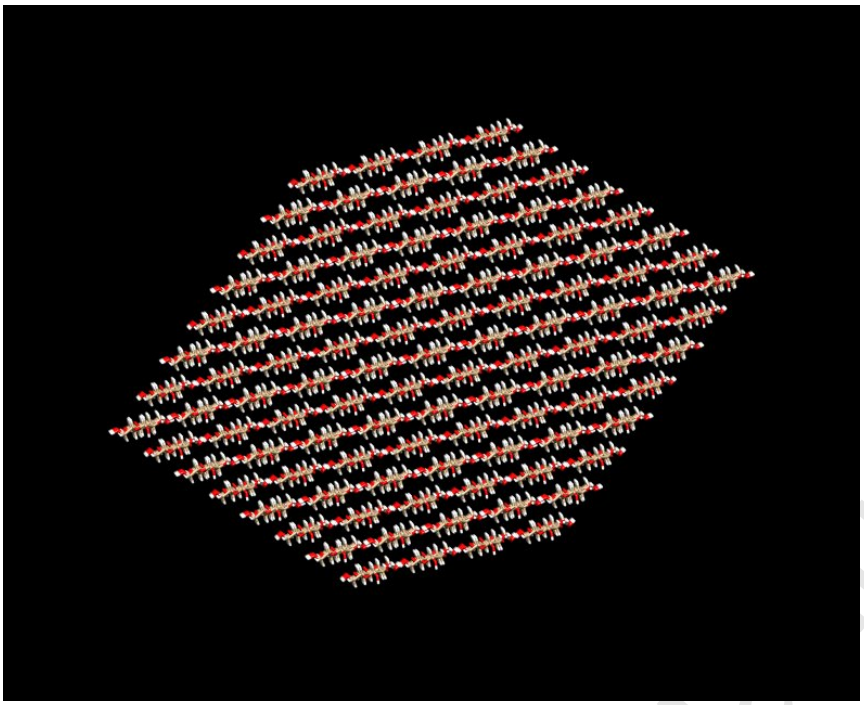

Figure 2

A model was constructed (Fig. 2) to have a width of 58.5 Å and, based on this model, a powder diffraction pattern was calculated in Fig. 3. Compared with the experimental pattern for the *of CCN-(O-C(O) Gly-NHC(O))Succinyl)-Ala-Ala-Pro-Val-AMC* (tetrapeptide-derivatized CCN, analog 2, Figure 1), there are important similarities and interesting differences. The peak positions and widths overlap quite well, but there is a disparity in the height of the background, especially in the 18° 2-θ region. Also, there are strong oscillations in the background. The higher background on the experimental pattern can be attributed to the added scattering from the unorganized peptide in the sample, and the oscillations can be attributed to a model having a finite size, which would lead to small-angle scattering. On the other hand, the basic crystal model seems to be a fair approximation to what might be observed in terms of its size and internal structure.

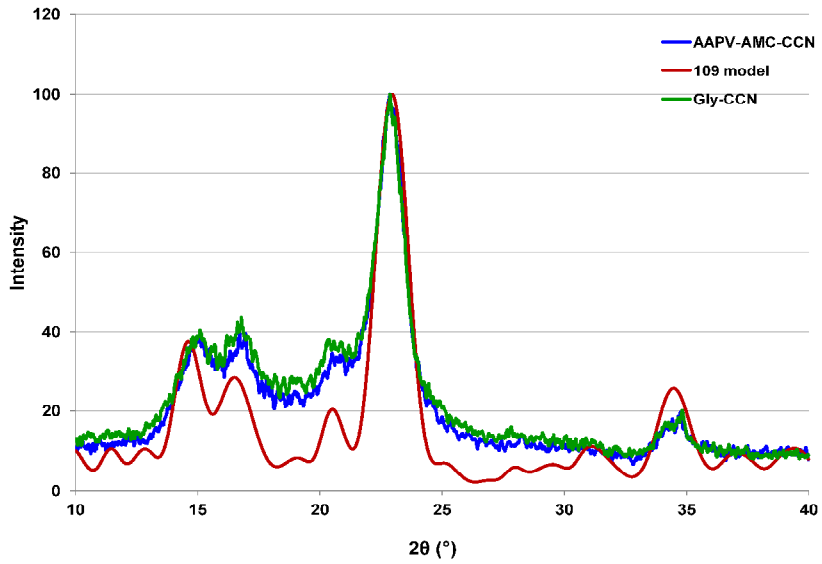

Figure 3

3.2 Kinetic Profiles

The kinetic parameters for the HNE and PPE hydrolyses of the tri- and tetrapeptide CCN analogs are shown in Table 2 and were derived from the reaction progress curves shown in Figure 4 and compared with substrate concentrations in solution at 0.5 U/mL HNE. The linearity of response of the kinetic measurements between the ranges of elastase substrate concentrations for both HNE and PPE are demonstrated by the correlation coefficients for Lineweaver Burke plots (1/v versus 1/[S]) and are close to 1.0 for all of the substrate analogs assayed (Table 2).

Table 2: Kinetic Parameters for the human neutrophil and porcine pancreatic elastase catalyzed hydrolysis of both fluorogenic peptide substrates[a]

Sample Description	k_{cat} (s^{-1})	K_m (μM)	k_{cat}/K_m ($M^{-1} \cdot s^{-1}$)	V_{max} (s^{-1})	Corr. Coeff.[b]
human neutrophil elastase					
Suc-APA-AMC in soln	3.858	596.4	6468.81	3.279	0.9928
Suc-APA-AMC on CCN	0.7732	23.07	33515.39	0.6572	0.9956
Suc-AAPV-AMC free in soln	21.13	256.4	82410.30	17.96	0.9976
Suc-AAPV-AMC on CCN	11.34	482.7	23492.85	9.637	0.9992
porcine pancreatic elastase					
Suc-APA-AMC free in soln	13.87	176.4	78628.12	16.64	0.9988
Suc-APA-AMC on CCN	6.644	922.4	7202.95	7.973	0.9928

[a] Conditions: Sodium phosphate buffer solution 0.1M with 0.5M NaCl at pH 7.6, 37ºC. The concentration of Human Neutrophil elastase was 0.5U/mL or 0.85μM and porcine pancreatic elastase was 0.5Units/mL or 1.2μM. [b] Correlation coefficients (Pearson r) using of the lineweaver-burke plot $1/v_o$ ($^{s-}1$) vs. 1/[S] in μM.

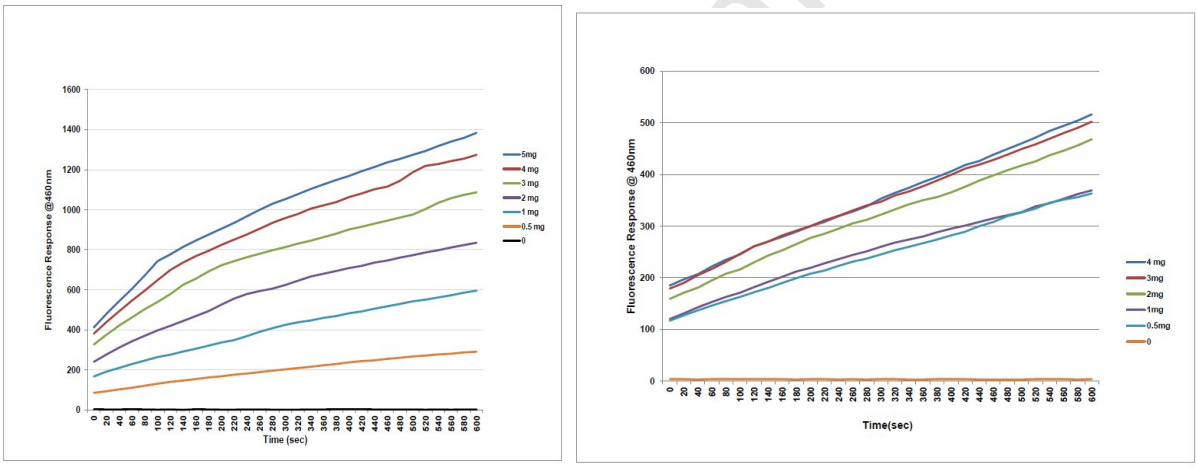

Figure 4

In Table 2, k_{cat} values for the substrate attached to the cellulose nanocrystalline matrix are listed. The k_{cat} value refers to the turnover rate or rate of product formation from reaction between enzyme and substrate elastase; a measurement of the rate of formation of hydrolyzed fluorophore (AMC) from the COOH-terminus of the CCN-bound peptide (Figure 1). The 2-5 fold higher k_{cat} values observed for the peptide substrates in solution compared with the peptide-CCN conjugates reflect a generally slower rate of product formation when the enzyme substrates are attached to the nanocrystalline cellulose. This is understandable in light of the two-phase reaction that is occurring

between the elastase and the peptide that is bound to the nanocrystal. The lower Vmax value, which is the maximum reaction rate mediated by the enzyme, observed for the peptide-CCN conjugates is consistent with the enzyme turnover rate decreasing in the conjugates. On the other hand the enzyme-substrate affinity or ability of the substrate to bind to the enzyme active site, as reflected in the K_m values, was variable. For example, the affinity of the tetrapeptide-CCN for HNE was 2-fold greater in solution than when it is covalently bound to CCN, and the tripeptide affinity for PPE was 5-fold greater in solution than when bound to CCN. However, the tripeptide substrate affinity for HNE when bound to CCN was 23-fold greater than the tripeptide substrate-HNE affinity in solution. Thus, the higher HNE affinity for the substrate tripeptide-CCN (Figure 1, R_2) also gives rise to a higher enzyme efficiency as seen by the higher k_{cat}/K_m assigned to CCN-(O-C(O) Gly-NHC(O))Succinyl)-Ala-Pro-Ala-AMC; it is 5-fold higher than the k_{cat}/K_m for the analogous enzyme substrate assessed in solution. Thus, the tripeptide-CCN performs better because of enhanced sensitivity to detection of HNE, compared to the analogous analog in solution. However, with PPE the efficiency of the tripeptides-CCN analog is 10-fold less than when it is freely dissolved in solution.

The elastase sensor limits of sensitivity at 2 mg of peptide-CCN substrate were assessed as previously reported (Edwards, Prevost, Sethumadhavan, Ullah & Condon, 2013) to compare the performance of the analogs of this study with previous detection limits. It was found that 2 mg of tripeptide-CCN could detect 0.03 U/mL PPE activity within a one hour time course by monitoring the change in fluorescence with analog 2, and 2 mg of tetrapeptide-CCN (analog 1, Figure 1) could detect HNE at 0.05 U/mL over a 15 minute time course. Since the concentrations of elastase substrates were considerably below the K_m values, it is expected that the sensor could improve limits of sensitivity at least four-fold down to 0.0075 U/mL which is in the low nanogram/mL range. This is consistent with previous reports that state that 0.33 and 0.47 ng/mL levels of HNE and PPE, i.e., picomolar concentration of the enzyme, can be detected with MeO-Suc-Ala-Ala-Pro-Val-AMC(Castillo, Nakajima, Zimmerman & Powers, 1979).

The fluorogenic substrate kcat/Km values are 11 and 2.5 times lower than the corresponding values for the colorimetric analog, which we have previously reported on CCN (Edwards, Prevost, Sethumadhavan, Ullah & Condon, 2013). However the highly fluorescent H-AMC chromophore makes the Suc-Ala-Ala-Pro-Val-AMC more sensitive to the detection of elastase than the peptidyl-4-paranitroanilide analog.

3.3 Structure Function Considerations

The depiction of a molecular model of the peptide-cellulose nanocrystal shown in Figure 5 portrays a putative conformational orientation of the anhydroglucose-hydroxymethyl-linked peptide in relation to the nanocrystalline surface and is substituted based on the stoichiometry observed in this study. The model portrays a minimized tetrapeptide with

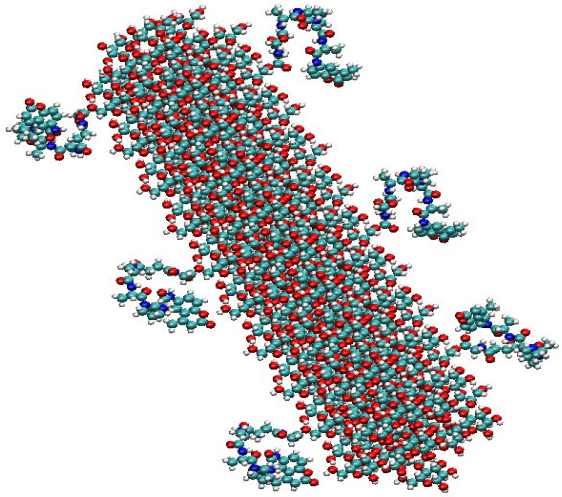

Figure 5

the structure of the tetrapeptide-linked cellulose conjugate in Figure 1, and it is linked to cellulose chains that are stacked in the structure of a small cellulose crystallite based on structural models of cellulose I structures. The turn conformation inherent to the peptide sequence (Marcelino & Gierasch, 2008) orients the COOH-terminal fluorophore in a seemingly parallel alignment to the surface of the cellulose nanocrystal. This apparent relation of the peptide to the cellulose crystallite surface when placed in a turn conformation may account in part for the difference in activity between the tri- and

tetrapeptides observed in this study. The tripeptide-cellulose conjugate as discussed above showed greater enzyme affinity than the tetrapeptide for HNE. Thus the orientation portrayed in the molecular model suggests relative turn contribution differences to elastase affinity for the tetrapeptide-conjugate, and previously Ala-Pro-Val has been identified as being uniquely a β-turn based on NMR-assigned torsion angles (Kleinpeter, Ströhl & Peinze, 1995). Hence this feature of the tripeptide may work synergistically with the cellulose chain and crystallite surface to contribute to the higher affinity of the cellulose bound tripeptide for HNE. However, other surface properties of the nanocrystals may also play a role in the activity of the tetrapeptide and tripeptide conjugates. The nanocrystalline surface is negatively charged and the positively charged elastase may directly bind to the nanocrystalline surface to enhance affinity of the enzyme for the cellulose bound peptide substrate.

4. Conclusions

The structure function relationship of a peptide-cellulose conjugate prepared on a cellulose nanocrystalline surface has been outlined here. The study demonstrates interesting activity and structural properties of an elastase biosensor that show how the attachment of peptides on cellulose nanocrystalline surfaces can be highly effective sensors. The peptide's disposition to protease binding are illustrated here both in the context of crystallite size and conformation of the peptide relative to the surface of the cellulose crystallite as is related to enhanced efficiency over enzyme activity typically found in solution. This paper definitively outlines the synthesis, characterization and activity of a peptide-cellulose conjugate that shows robust and sensitive activity with potential as point of care diagnostic use for chronic diseases where human neutrophil elastase and pancreatic elastase biomarkers.

References

Araújo, A. C., Nakhai, A., Ruda, M., Slättegård, R., Gatenholm, P., & Brumer, H. (2012). A general route to xyloglucan-peptide conjugates for the activation of cellulose surfaces. *Carbohydrate Research, 354*(0), 116-120.

534 Azizi Samir, M. A. S., Alloin, F., Sanchez, J.-Y., El Kissi, N., & Dufresne, A. (2004).
535 Preparation of Cellulose Whiskers Reinforced Nanocomposites from an Organic
536 Medium Suspension. *Macromolecules, 37*(4), 1386-1393.
537 Ballerstadt, R., & Schultz, J. S. (1996). Sensor methods for use with microdialysis and
538 ultrafiltration. *Advanced Drug Delivery Reviews, 21*(3), 225-238.
539 Barazzouk, S., & Daneault, C. (2012). Amino Acid and Peptide Immobilization on
540 Oxidized Nanocellulose: Spectroscopic Characterization. *Nanomaterials, 2*(2),
541 187-205.
542 Blackwell, H. E. (2006). Hitting the SPOT: small-molecule macroarrays advance
543 combinatorial synthesis. *Current Opinion in Chemical Biology, 10*(3), 203-212.
544 Bode, W., Meyer, E., Jr., & Powers, J. C. (1989). Human leukocyte and porcine
545 pancreatic elastase: X-ray crystal structures, mechanism, substrate specificity,
546 and mechanism-based inhibitors. *Biochemistry, 28*(5), 1951-1963.
547 Boudjelthia, A. K., Saulnier, J., & Wallach, J. M. (1990). Elastolysis of kappa-elastin
548 sub-fractions by pancreatic and leukocyte elastases. *Biochem Int, 21*(1), 145-
549 153.
550 Caielli, S., Banchereau, J., & Pascual, V. (2012). Neutrophils come of age in chronic
551 inflammation. *Curr Opin Immunol, 24*(6), 671-677.
552 Castillo, M. J., Nakajima, K., Zimmerman, M., & Powers, J. C. (1979). Sensitive
553 substrates for human leukocyte and porcine pancreatic elastase: A study of the
554 merits of various chromophoric and fluorogenic leaving groups in assays for
555 serine proteases. *Analytical Biochemistry, 99*(1), 53-64.
556 Das, G., Talukdar, P., & Matile, S. (2002). Fluorometric detection of enzyme activity with
557 synthetic supramolecular pores. *Science, 298*(5598), 1600-1602.
558 Edwards, J. V., Prevost, N., Sethumadhavan, K., Ullah, A., & Condon, B. (2013).
559 Peptide conjugated cellulose nanocrystals with sensitive human neutrophil
560 elastase sensor activity. *Cellulose, 20*(3), 1223-1235.
561 Eyley, S., & Thielemans, W. (2011). Imidazolium grafted cellulose nanocrystals for ion
562 exchange applications. *Chemical Communications, 47*(14), 4177-4179.
563 Filpponen, I., Sadeghifar, H., & Argyropoulos, D. S. (2011). Photoresponsive cellulose
564 nanocrystals. *Nanomaterials and Nanotechnology, 1*(1), 34-43.
565 Fleming, K., Gray, D. G., & Matthews, S. (2001). Cellulose Crystallites. *Chemistry – A
566 European Journal, 7*(9), 1831-1836.
567 Habibi, Y., Chanzy, H., & Vignon, M. (2006). TEMPO-mediated surface oxidation of
568 cellulose whiskers. *Cellulose, 13*(6), 679-687.
569 Hassan, M. L., Moorefield, C. M., Elbatal, H. S., Newkome, G. R., Modarelli, D. A., &
570 Romano, N. C. (2012). Fluorescent cellulose nanocrystals via supramolecular
571 assembly of terpyridine-modified cellulose nanocrystals and terpyridine-modified
572 perylene. *Materials Science and Engineering: B, 177*(4), 350-358.
573 Henares, T. G., Takaishi, M., Yoshida, N., Terabe, S., Mizutani, F., Sekizawa, R., &
574 Hisamoto, H. (2006). Integration of Multianalyte Sensing Functions on a
575 Capillary-Assembled Microchip: Simultaneous Determination of Ion
576 Concentrations and Enzymatic Activities by a “Drop-and-Sip” Technique.
577 *Analytical Chemistry, 79*(3), 908-915.
578 Humphrey, W., Dalke, A., & Schulten, K. (1996). VMD: Visual molecular dynamics.
579 *Journal of Molecular Graphics, 14*(1), 33-38.

580 Jaffray, C., Yang, J., Carter, G., Mendez, C., & Norman, J. (2000). Pancreatic elastase
581 activates pulmonary nuclear factor kappa B and inhibitory kappa B, mimicking
582 pancreatitis-associated adult respiratory distress syndrome. *Surgery, 128*(2),
583 225-231.
584 Jiang, F., Han, S., Hsieh, Y.-L. (2013) Controlled defibrillation of rice straw cellulose and
585 self-assembly of cellulose nanofibrils into highly crystalline fibrous materials,
586 R.S.C. Advances, (3), 12366-12375.
587 Kleinpeter, E., Ströhl, D., & Peinze, S. (1995). Solution conformation of tripeptides by
588 NMR spectroscopy and force-field calculations. *Structural Chemistry, 6*(6), 377-
589 382.
590 Korkmaz, B., Attucci, S., Epinette, C., Pitois, E., Jourdan, M.-L., Juliano, L., & Gauthier,
591 F. (2012). Measurement of Neutrophil Elastase, Proteinase 3, and Cathepsin G
592 Activities using Intramolecularly Quenched Fluorogenic Substrates. In R. B.
593 Ashman (Ed.). *Leucocytes* (Vol. 844, pp. 125-138): Humana Press.
594 Korkmaz, B., Horwitz, M. S., Jenne, D. E., & Gauthier, F. (2010). Neutrophil elastase,
595 proteinase 3, and cathepsin G as therapeutic targets in human diseases.
596 *Pharmacol Rev, 62*(4), 726-759.
597 Lam, E., Male, K. B., Chong, J. H., Leung, A. C. W., & Luong, J. H. T. (2012).
598 Applications of functionalized and nanoparticle-modified nanocrystalline
599 cellulose. *Trends in Biotechnology, 30*(5), 283-290.
600 Leegsma-Vogt, G., Rhemrev-Boom, M. M., Tiessen, R. G., Venema, K., & Korf, J.
601 (2004). The potential of biosensor technology in clinical monitoring and
602 experimental research. *Bio-Medical Materials and Engineering, 14*(4), 455-464.
603 Macrae, C. F., Bruno, I. J., Chisholm, J. A., Edgington, P. R., McCabe, P., Pidcock, E.,
604 Rodriguez-Monge, L., Taylor, R., van de Streek, J., & Wood, P. A. (2008).
605 Mercury CSD 2.0 - new features for the visualization and investigation of crystal
606 structures. *Journal of Applied Crystallography, 41*(2), 466-470.
607 Mahmoud, K. A., Mena, J. A., Male, K. B., Hrapovic, S., Kamen, A., & Luong, J. H. T.
608 (2010). Effect of Surface Charge on the Cellular Uptake and Cytotoxicity of
609 Fluorescent Labeled Cellulose Nanocrystals. *ACS Applied Materials & Interfaces,*
610 *2*(10), 2924-2932.
611 Marcelino, A. M. C., & Gierasch, L. M. (2008). Roles of β-turns in protein folding: From
612 peptide models to protein engineering. *Biopolymers, 89*(5), 380-391.
613 McRae, B., Nakajima, K., Travis, J., & Powers, J. C. (1980). Studies on reactivity of
614 human leukocyte elastase, cathepsin G, and porcine pancreatic elastase toward
615 peptides including sequences related to the reactive site of .alpha.1-protease
616 inhibitor (.alpha.1-antitrypsin). *Biochemistry, 19*(17), 3973-3978.
617 Nishiyama, Y., Johnson, G., & French, A. (2012). Diffraction from nonperiodic models of
618 cellulose crystals. *Cellulose, 19*(2), 319-336.
619 Nishiyama, Y., Langan, P., & Chanzy, H. (2002). Crystal Structure and Hydrogen-
620 Bonding System in Cellulose Iβ from Synchrotron X-ray and Neutron Fiber
621 Diffraction. *Journal of the American Chemical Society, 124*(31), 9074-9082.
622 Okita, Y., Saito, T., Isogai, A., (2010). Entire surface oxidation of various cellulose
623 microfibrils by tempo-mediated oxidation. Biomacromolecules, 11, 1696-1700.

Scherrer, P. (1918). Bestimmung der Grösse und der inneren Struktur von Kolloidteilchen mittels Röntgenstrahlen. *Nachrichten von der Köngl. Gesellschaft der Wissenschaften zu Göttingen, Mathematisch-Physikalische Klasse 2*, 98-100.

Segal, L., Creely, J. J., Martin, A. E., & Conrad, C. M. (1959). An Empirical Method for Estimating the Degree of Crystallinity of Native Cellulose Using the X-Ray Diffractometer. *Textile Research Journal, 29*(10), 786-794.

Shen, B., Shimmon, S., Smith, M. M., & Ghosh, P. (2003). Biosensor analysis of the molecular interactions of pentosan polysulfate and of sulfated glycosaminoglycans with immobilized elastase, hyaluronidase and lysozyme using surface plasmon resonance (SPR) technology. *J Pharm Biomed Anal, 31*(1), 83-93.

Siqueira, G., Bras, J., & Dufresne, A. (2009). New Process of Chemical Grafting of Cellulose Nanoparticles with a Long Chain Isocyanate. *Langmuir, 26*(1), 402-411.

Sorde, N., Das, G., & Matile, S. (2003). Enzyme screening with synthetic multifunctional pores: focus on biopolymers. *Proc Natl Acad Sci U S A, 100*(21), 11964-11969.

Stein, R. L. (1983). Catalysis by human leukocyte elastase: substrate structural dependence of rate-limiting protolytic catalysis and operation of the charge relay system. *Journal of the American Chemical Society, 105*(15), 5111-5116.

Steuerwald, A. J., Villeneuve, J. D., Sun, L., & Stenken, J. A. (2006). In vitro characterization of an in situ microdialysis sampling assay for elastase activity detection. *J Pharm Biomed Anal, 40*(5), 1041-1047.

Subirós-Funosas, R., Prohens, R., Barbas, R., El-Faham, A., & Albericio, F. (2009). Oxyma: An Efficient Additive for Peptide Synthesis to Replace the Benzotriazole-Based HOBt and HOAt with a Lower Risk of Explosion[1]. *Chemistry – A European Journal, 15*(37), 9394-9403.

Touzinsky, G. F., & Gordon, S. M. (1979). Degree of substitution of cellulose derivatives containing n different substituent groups. *Carbohydrate Research, 69*(1), 327-329.

Weiss, S. J. (1989). Tissue destruction by neutrophils. *N Engl J Med, 320*(6), 365-376.

Yang, Q., & Pan, X. (2010). A facile approach for fabricating fluorescent cellulose. *Journal of Applied Polymer Science, 117*(6), 3639-3644.

Yasutake, A., & Powers, J. C. (1981). Reactivity of human leukocyte elastase and porcine pancreatic elastase toward peptide-4-nitroanilides containing model desmosine residues. Evidence that human leukocyte elastase is selective for crosslinked regions of elastin. *Biochemistry, 20*(13), 3675-3679.

Yue, Y., Zhou, C, French, A.D., Xia, G, Han, G., Wang, Q., Wu, Q., (2012). Comparative properties of cellulose nanocrystals from native and mercerized cotton fibers. Cellulose, 19: 1173-1187.

Acknowledgments: The authors wish to thank Professor Qinglin Wu, Louisiana State University for providing cotton cellulose nanocrystals used in this study.

Figure Legends:

Figure 1: *Structure of CCN-(O-C(O) Gly-NHC(O))Succinyl)-Ala-Ala-Pro-Val-AMC (R_1 analog)* and CCN-(O-C(O) Gly-NHC(O))Succinyl)-Ala-Pro-Ala-AMC (R_2 analog), where cellotetraose structure represents the adjoining cellulose chain of the cotton cellulose nanocrystal.

Figure 2: Constructed model of a cellulose crystal based on the x-ray diffraction pattern seen in Figure 4. The width is 58.5 Angstroms.

Figure 3: X-ray diffraction spectra of both CCN-(O-C (O)-Gly [green] and CCN-(O-C(O) Gly-NHC(O))Succinyl)-Ala-Ala-Pro-Val-AMC [blue] in addition to the simulated pattern of a powder diffraction pattern based on the model constructed for the cellulose crystal shown in Figure 2 [red].

Figure 4: Reaction progress curves for A) various amounts of nanocrystalline cellulose with immobilized tripeptide (CCN-(O-C(O) Gly-NHC(O))Succinyl)-Ala-Pro-Ala-AMC) reacted with 0.5U/mL of porcine pancreatic elastase @ 37°C ; B) various amounts of nanocrystal with immobilized tripeptide (CCN-(O-C(O) Gly-NHC(O))Succinyl)-Ala-Pro-Ala-AMC) with 0.5U/mL of human neutrophil elastase @ 37°C.

Figure 5: Molecular model of cellulose crystal with conjugated peptide (CCN-(O-C (O) Gly-NHC (O))Succinyl)-Ala-Ala-Pro-Val-AMC (R_1 analog). The peptide-conjugated cellulose model was assembled and optimized as described in the Materials and Methods section.

- Cotton cellulose nanocrystals were conjugated to small fluorescent peptide.
- From a cellulose I x-ray diffraction pattern a crystallite size of 58.5 Å was calculated.
- A tripeptide conjugate has enhanced efficiency in human neutrophil elastase recognition.
- The peptide-cellulose nanocrystals demonstrate sensitive fluorescent elastase detection.
- A peptide-cellulose nanocrystal model consistent with degree of substitution levels was built.